A Tyrosine Kinase Inhibitor–Based High-Affinity PET Radiopharmaceutical Targets Vascular Endothelial Growth Factor Receptor

Feng Li[1], Sheng Jiang[2], Youli Zu[3], Daniel Y. Lee[1], and Zheng Li[1]

[1]Department of Translational Imaging, Houston Methodist Research Institute, Weill Cornell Medical College, Houston, Texas; [2]Laboratory of Medicinal Chemistry, Guangzhou Institute of Biomedicine and Health, Chinese Academy of Sciences, Guangzhou, China; and [3]Department of Pathology and Genomic Medicine, Houston Methodist Research Institute, Weill Cornell Medical College, Houston, Texas

Tyrosine kinase receptors including vascular endothelial growth factor receptor (VEGFR) have gained significant attention as pharmacologic targets. However, clinical evaluation of small-molecule drugs or biologics that target these pathways has so far yielded mixed results in a variety of solid tumors. The reasons for response variability remain unknown, including the temporal and spatial patterns of receptor tyrosine kinase expression. Methods to detect and quantify the presence of such cellular receptors would greatly facilitate drug development and therapy response assessment. We aimed to generate specific imaging agents as potential companion diagnostics that could also be used for targeted radionuclide therapy. Here, we report on the synthesis and initial preclinical performance of ^{64}Cu-labeled probes that were based on the kinase inhibitor already in clinical use, vandetanib (ZD6474), as a VEGFR-selective theranostic radiopharmaceutical. **Methods:** A monomeric (ZD-G1) and a dimeric (ZD-G2) derivative of ZD6474 were synthesized and conjugated with DOTA for chelation with ^{64}Cu to produce the probes ^{64}Cu-DOTA-ZD-G1 and ^{64}Cu-DOTA-ZD-G2. The binding affinity and specificity to VEGFR were measured using U-87 MG cells known to overexpress VEGFR. Small-animal PET and biodistribution studies were performed with ^{64}Cu-labeled probes (3–4 MBq) intravenously administered in U-87 MG tumor–bearing mice with or without coinjection of unlabeled ZD-G2 for up to 24 h after injection. **Results:** Receptor-binding assays yielded a mean equilibrium dissociation constant of 44.7 and 0.45 nM for monomeric and dimeric forms, respectively, indicating a synergistic effect in VEGFR affinity by multivalency. Small-animal PET/CT imaging showed rapid tumor accumulation of ^{64}Cu-DOTA-ZD-G2, with excellent tumor–to–normal tissue contrast by 24 h. Coinjection of the ^{64}Cu-DOTA-ZD-G2 with 50 nmol (60 μg) of nonradioactive ZD-G2 effectively blocked tumor uptake. **Conclusion:** A ^{64}Cu-labeled probe derived from an approved oncologic drug selective for VEGFR demonstrates excellent tumor targeting, particularly for the dimeric form. The multivalent probe yielded a 100-fold improvement in receptor affinity while maintaining pharmacokinetic and biodistribution properties well suited for PET imaging in our preclinical model. These results indicate that a clinically relevant theranostic platform can be rapidly developed from known small molecules that target key cellular receptors.

Key Words: vascular endothelial growth factor receptor (VEGFR); tumor angiogenesis; ^{64}Cu; theranostic

J Nucl Med 2014; 55:1525–1531
DOI: 10.2967/jnumed.114.138925

Vascular endothelial growth factors (VEGFs) are critical regulators of vasculogenesis and angiogenesis by binding to their cognate receptor, VEGFR (*1–6*). Stimulation of VEGFR results in endothelial cell proliferation, migration, and inhibition of apoptosis (*7–10*). Several antitumor drugs that target VEGF signaling have been approved by the Food and Drug Administration including bevacizumab and several receptor tyrosine kinase inhibitors such as pazopanib and vandetanib (ZD6474; Caprelsa [AstraZeneca]) (*11,12*). Other drugs targeting VEGF/VEGFR continue to be explored at the preclinical stage, and some have reached clinical trials (*13,14*). Despite promising results, the overall response rate for this class of drugs is highly variable (*15*). Although these drugs target specific receptors, the temporal and spatial expression patterns of those receptors are largely unknown in vivo, which may, in part, contribute to the observed variability in clinical outcome. Methods to detect and quantify the presence of such cellular receptors would greatly facilitate targeted drug development and therapy response assessment.

Molecular imaging agents that target VEGF/VEGFR have recently been used to diagnose and monitor the proliferation and development of angiogenic tumors (*16–19*). VEGF/VEGFR antibodies have been labeled with various radioisotopes for the imaging of VEGFR expression in various disease models (*20*). For example, extracellular VEGF imaging was accomplished by coupling anti-VEGF monoclonal antibodies (bevacizumab, HuMV833) with ^{89}Zr (*21,22*), ^{111}In (*23*), and ^{124}I (*24*). Recombinant $VEGF_{165}$ was efficiently labeled with ^{123}I and $VEGF_{121}$ with both ^{99m}Tc and ^{64}Cu for VEGF imaging in preclinical models (*25–28*). In the reported studies, successful visualization of VEGFR expression was demonstrated; however, low to moderate tumor-to-background ratios were obtained despite the high receptor affinity of these probes. Moreover, these biologics-based imaging agents may perform suboptimally in the clinical setting because of their slow clearance and nonspecific biodistribution (*16*). Small-molecule imaging probes are favored over biologics because of faster specific binding to target receptors, higher clearance rate, metabolic stability, and lower nonspecific background

Received Feb. 11, 2014; revision accepted May 6, 2014.
For correspondence or reprints contact: Zheng Li, Houston Methodist Research Institute, 6670 Bertner St., Houston, TX 77030.
E-mail: zli@houstonmethodist.org
Published online Jun. 26, 2014.

signal. Furthermore, the radiolabeling chemistry and purification procedures for small molecules are often less laborious and fully scalable for commercial production. We took the small-molecule approach to develop a VEGFR-specific imaging agent that would also serve as a candidate theranostic platform amenable to rapid clinical translation.

Vandetanib is an orally bioavailable antiangiogenic quinazoline drug selective for the tyrosine kinase activity of vascular endothelial growth factor receptor 2 (VEGFR2) with a 50% inhibitory concentration value of 40 nM (*15*). It was the first drug to be approved by the Food and Drug Administration for the treatment of progressive advanced medullary thyroid cancer in adult patients. It was also shown to inhibit the growth of experimental lung metastases (*29*). Vandetanib was also radiolabeled with ^{11}C to generate a PET radiopharmaceutical analog for VEGFR2 imaging; however, its uptake in subcutaneous tumors in preclinical models was suboptimal (*30*). On the basis of our prior experience with strategies to enhance target affinity of chemical probes (*31*), we leveraged the known structure selectivity relationship of vandetanib to optimize this parent compound for PET imaging using a multivalent approach.

MATERIALS AND METHODS

Chemistry and Radiolabeling

Second-generation ZD-G2 was synthesized from triethylamine and ZD-G1 in 2 steps (supplemental data [supplemental materials are available at http://jnm.snmjournals.org]). DOTA conjugation to ZD-G1 and ZD-G2 was performed as follows. DOTA-*N*-hydroxysuccinimide (NHS)-ester (3 mg, 6 μmol) was added to 0.5 mL of ZD-G2 dimethyl sulfoxide solution (10 μmol/mL; 6 μmol), and then 50 μL of triethylamine were added. The reaction mixture was stirred in the dark at ambient temperature overnight and then quenched by adding 200 μL of trifluoroacetic acid. The crude product was purified by semipreparative reversed-phase high-performance liquid chromatography (HPLC) using a Phenomenex Luna C-18 column (250 × 10 mm). Fractions containing ZD-G2-DOTA were collected, lyophilized, and stored in the dark at −20°C until use. ZD-G1-DOTA was prepared using procedures similar to those described above. The purified ZD-G1-DOTA and ZD-G2-DOTA were characterized by mass spectroscopy (MS). MS (ZD-G1-DOTA, electrospray): *m/z* 847.3($[M+H]^+$, calculated 846.27); 424.3 ($[M+2H]^{2+}$). MS (ZD-G2-DOTA, electrospray): *m/z* 1,596.32($[M+H]^+$, calculated 1,596.3); 789.6 ($[M+2H]^{2+}$).

ZD-G2-DOTA and ZD-G1-DOTA were radiolabeled using procedures described in our previously published report (*32*). Briefly, 185 MBq (5 mCi) of $^{64}CuCl_2$ in 0.1 M HCl were diluted by adding 300 μL of 0.1 M ammonium acetate (pH 5.6). ZD-G1-DOTA or ZD-G2-DOTA (10 μmol/mL, 100 nmol) in 700 μL of 0.1 M ammonium acetate was mixed with approximately 37–74 MBq (1–2 mCi) of $^{64}Cu(OAc)_2$. The mixture was stirred and incubated at 50°C for 1 h. ^{64}Cu-labeled compound was purified by semipreparative radio-HPLC, and the collected fraction containing ^{64}Cu-DOTA-ZD-G2 or ^{64}Cu-DOTA-ZD-G1 was evaporated and reconstituted in phosphate-buffered saline (PBS), which was filtered into a sterile dose vial by passing through a 0.22-μm filter (Millipore). The radiochemical yield and chemical purity were determined by HPLC. The stability of ^{64}Cu-DOTA-ZD-G1 and ^{64}Cu-DOTA-ZD-G2 (370 kBq/100 μL) was also evaluated by incubating in Dulbecco modified Eagle medium (DMEM; Invitrogen) containing 10% fetal bovine serum and mouse serum at 37°C for up to 24 h. Aliquots at 2, 6, and 24 h were analyzed by HPLC and radio–thin-layer chromatography.

Cell Lines and Animal Model

U-87 MG human glioblastoma cells, MDA-MB-231 human breast cancer cells, and HeLa cells were purchased from the American Type Culture Collection and grown in DMEM with 10% fetal bovine serum at 37°C with 5% CO_2. Human umbilical vein endothelial cells (HUVEC) were purchased from PromoCell and cultured in endothelial cell growth medium (Ready-to-use; PromoCell). Cells were used for in vitro and in vivo experiments when they reached approximately 75% confluence. All animal experiments were performed under approved protocols in compliance with the guidelines established by the Institutional Animal Care and Use Committee (IACUC) of the Houston Methodist Research Institute. Five-week-old female nude mice were purchased from Charles River. The U-87 MG xenograft model was generated by subcutaneous injection of 5×10^6 cells (suspended in 100 μL of PBS) into the left flank of each mouse. Three to 4 wk after inoculation (tumor volume, ∼200–500 mm^3), the mice were used for PET imaging and biodistribution studies. Mice were sacrificed by CO_2 asphyxiation and cervical dislocation per IACUC protocol.

Cell Uptake and Blocking Assay

The ^{64}Cu-DOTA-ZD-G2 cell uptake assay was performed using U-87 MG, MDA-MB-231, HeLa, and HUVECs that overexpress VEGFR to varying degrees as demonstrated by Western blot analysis (supplemental data). The day before the experiment, cells were seeded in 24-well plates at a concentration of 2×10^5 cells per well in the appropriate growth medium (see previous section). ^{64}Cu-DOTA-ZD-G2 (37 kBq [1 μCi]) was added to each well and incubated at 4°C for 1 h at a concentration of 80 nM in medium (200 μL/well). After incubation, cells were washed with ice-cold PBS 3 times and trypsinized. Cells were harvested into a microfuge tube and spun down at 1,500 rpm in a microcentrifuge. Cell pellet–associated radioactivity was measured using a γ counter (Perkin-Elmer Packard). ^{64}Cu-DOTA-ZD-G1 and ^{64}Cu-DOTA-ZD-G2 cell uptake and blocking assays were performed using U-87 MG cells following the same procedure described above. Briefly, 37 kBq of ^{64}Cu-DOTA-ZD-G1 or ^{64}Cu-DOTA-ZD-G2 in 200 μL of DMEM (non–fetal bovine serum) were added to each well without or with a 50-fold excess amount of nonradioactive ZD-G1 or ZD-G2, respectively. After incubation at 4°C for 1 h, cells were washed with ice-cold PBS and harvested for γ counting as described above.

Cell VEGFR-Binding Assay

VEGFR-binding affinity and specificity of the ^{64}Cu-DOTA-ZD-G1 or ^{64}Cu-DOTA-ZD-G2 were evaluated by saturation and displacement assays using U-87 MG cells. Detailed procedures are described in the supplemental data. Briefly, cells were seeded in 12-well plates at a density of 5×10^5 cells per well the day before the experiment. For receptor-saturation analyses, cells were incubated at 4°C for 1 h with increasing concentrations of ^{64}Cu-DOTA-ZD-G1 or ^{64}Cu-DOTA-ZD-G2 in culture medium. Cells were then washed with cold PBS, trypsinized, collected by centrifugation, and measured by γ counting. Mean equilibrium dissociation constant (K_d) values were calculated by nonlinear regression using GraphPad Prism (GraphPad Software). For displacement/competition assays, cells were incubated with ^{64}Cu-DOTA-ZD-G1 or ^{64}Cu-DOTA-ZD-G2 and increasing concentrations of nonradioactive ZD-G1 or ZD-G2, respectively. The experimental procedures were similar to those used for the saturation study described above. All experiments were performed in triplicate.

Small-Animal PET Imaging

Small-animal PET/CT scans were obtained and image analysis performed using the manufacturer's software platform (Inveon; Siemens). Approximately 3.7 MBq of ^{64}Cu-DOTA-ZD-G1 or ^{64}Cu-DOTA-ZD-G2 (100 μCi, 1.6–2.2 nmol) were injected intravenously through the tail vein of each mouse ($n = 5$). In-line PET and CT scans were acquired at 2, 6, and 24 h after injection, and images were obtained using the manufacturer's 2-dimensional ordered-subsets expectation maximum algorithm. PET/CT image fusion was performed with the Inveon Research Workplace. For each PET scan, regions of interest (ROIs) were drawn over the tumor and major organs on decay-corrected whole-body coronal images. The radioactivity concentration (accumulation) within tumor or organs was obtained from mean pixel values within the ROI volume and was converted to counts per milliliter per minute. Assuming a tissue density of 1 g/mL, the counts per milliliter per minute was converted to counts per gram per minute and then divided by the injected dose (ID) to obtain an imaging ROI–derived percentage of the injected radioactive dose per gram of tissue (%ID/g). A blocking experiment was performed by coinjection of ^{64}Cu-DOTA-ZD-G2 with nonradioactive ZD-G2 (50 nmol, 60 μg/mouse).

Biodistribution Study

After the final small-animal PET/CT scans at 24 h after injection, mice were immediately sacrificed to evaluate radiotracer biodistribution. Blood, tumor, heart, lungs, liver, spleen, kidneys, and muscle were collected and wet weighed. The radioactivity in each tissue was measured using a γ counter and expressed as %ID/g.

RESULTS

Synthesis and Radiochemistry

Bivalent ZD-G2 (Fig. 1) was synthesized by coupling the parent antiangiogenic drug ZD-G1 with 2 arms of active tricarbonylimidazole ester of triethanolamine and with ethylenediamine coupling with carbonylimidazole an ester group on the third arm. ZD-G1 and ZD-G2 were then reacted with DOTA-NHS ester to obtain ZD-G1-DOTA and ZD-G2-DOTA. The compounds were purified by HPLC and were characterized by MS. Yields for ZD-G1-DOTA and ZD-G2-DOTA were 85% and 72%, respectively.

In the radiolabeling reaction, ^{64}Cu-DOTA-ZD-G1 and ^{64}Cu-DOTA-ZD-G2 (Fig. 1) were obtained in 80%–90% decay-corrected yield, with a radiochemical purity of more than 98%. The specific activity of ^{64}Cu-DOTA-ZD-G1 and ^{64}Cu-DOTA-ZD-G2 was estimated to be 1.7–2.3 MBq/nmol. The chemical stability of each compound was evaluated by radio-HPLC analysis, which revealed no change in the chromatogram after 24-h incubation in tissue culture medium (DMEM containing 10% fetal bovine serum) and mouse serum at 37°C (supplemental data).

Cell Uptake and Blocking Study

The cell uptake study of ^{64}Cu-DOTA-ZD-G2 was performed using the cell lines U-87 MG, MDA-MB-231, HeLa, and HUVEC. Western blot was performed on these cell lines to determine the VEGFR2 expression using anti-VEGF-R^2/Flk-1 antibody (supplemental data). HUVECs demonstrate high VEGFR2 expression, U-87 cells have moderate expression, and both MDA-MB-231 and HeLa cells exhibit low expression. The radiotracer uptake levels as shown in Figure 2A also revealed the same relative order: HUVEC > U-87 > HeLa and MDA-MB-231 cells, in good agreement with the Western blot results. The comparison of ^{64}Cu-DOTA-ZD-G1 and ^{64}Cu-DOTA-ZD-G2 uptake using U-87 cells is shown in Figure 2B.

Cell VEGFR2-Binding Assay

The binding assay of the ^{64}Cu-DOTA-ZD-G1 and ^{64}Cu-DOTA-ZD-G2 to U-87 MG cells yielded a K_d value of 44.7 and 0.45 nM, respectively, representing a 100-fold-higher avidity of the dimeric construct over the monomeric form. The representative saturation curves of specifically bound ^{64}Cu-DOTA-ZD-G1 and ^{64}Cu-DOTA-ZD-G2 are shown in Figures 3A and 3B. Nonradioactive ZD-G2 effectively competes with ^{64}Cu-DOTA-ZD-G2 in a dose-dependent manner, as shown in Figure 3C, providing strong evidence for specific VEGFR2 targeting. Similar results were obtained in competition assays with ^{64}Cu-DOTA-ZD-G1 and cold ZD-G1. The calculated 50% inhibitory concentration values for ZD-G1 and ZD-G2 were 17.63 ± 1.2 and 0.023 ± 0.002 nM, respectively.

Small-Animal PET/CT Imaging

Multiple time-point small-animal PET/CT scans of ^{64}Cu-DOTA-ZD-G1 and ^{64}Cu-DOTA-ZD-G2 were obtained using U-87 MG tumor–bearing nude mice (*n* = 5 per group). Representative decay-corrected coronal images at 2, 6, and 24 h after injection are shown in Figure 4. Images revealed detectable radiotracer accumulation at tumor sites as early as 2 h after injection. Consistent with the in vitro results, ^{64}Cu-DOTA-ZD-G2 showed significantly greater tumor uptake than ^{64}Cu-DOTA-ZD-G1 at all time points examined. From the ROI analysis displayed in Figure 6A, tumor uptake reached 2.70 ± 0.06 %ID/g at 2 h, 3.83 ± 0.26 %ID/g at 6 h, and 3.84 ± 0.05 %ID/g at 24 h after injection of ^{64}Cu-DOTA-ZD-G2. For the monomeric probe, ^{64}Cu-DOTA-ZD-G1, tumor uptake was 0.27 ± 0.06 %ID/g at 2 h, 0.64 ± 0.02 %ID/g at 6 h, and 0.46 ± 0.06 %ID/g at 24 h after injection, representing more than 5-times-higher tumor uptake of the dimeric probe ($P < 0.0001$). Semiquantitative analysis showed high tumor-to-muscle uptake of ^{64}Cu-DOTA-ZD-G2 as shown in Figure 6B. Interestingly, ^{64}Cu-DOTA-ZD-G2 exhibited high liver uptake at early time points, with low distribution in kidneys and other tissues (Figs. 6C and 6D). At 24 h after injection, liver uptake decreased to 3.94 ± 1.07 %ID/g, compared with tumor uptake at 3.84 ± 0.05 %ID/g. To assess VEGFR specificity in vivo, we performed blocking experiments by coinjection of 50 nmol (60 μg/animal) of nonradioactive ZD-G2 and ^{64}Cu-DOTA-ZD-G2. Tumor activity was effectively reduced at all time

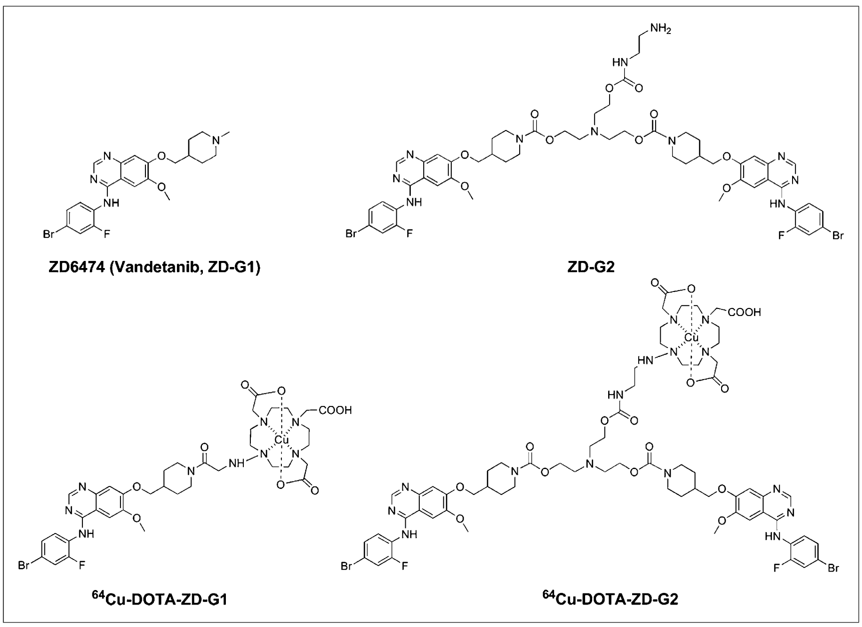

FIGURE 1. Chemical structures of ZD6474 (ZD-G1), ZD-G2, ^{64}Cu-DOTA-ZD-G1, and ^{64}Cu-DOTA-ZD-G2.

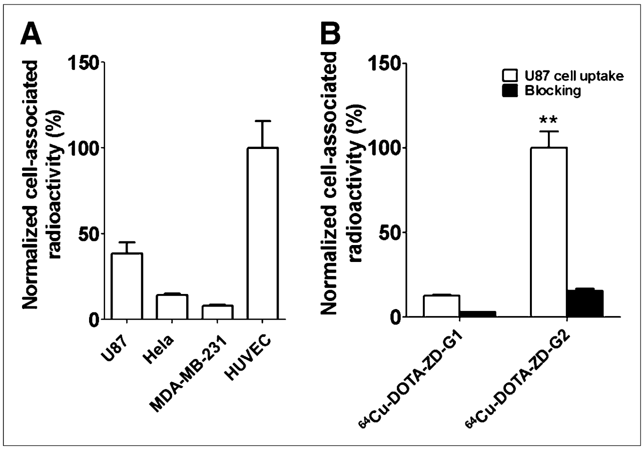

FIGURE 2. Cell uptake and competition assay. (A) Binding of ^{64}Cu-DOTA-ZD-G2 to cells with varying levels of VEGFR2. (B) Comparison of cell binding with ^{64}Cu-DOTA-ZD-G2 and ^{64}Cu-DOTA-ZD-G1 in U-87 cells. Competitive blocking with nonradioactive ZD-G2 and ZD-G1, respectively. (n = 3, **P < 0.0001).

points by PET imaging (Fig. 5), with radiotracer uptake values of 0.57 ± 0.01 %ID/g at 2 h, 0.63 ± 0.07 %ID/g at 6 h, and 0.92 ± 0.21 %ID/g at 24 h after injection (Fig. 6A). These results indicate significantly improved specific VEGFR binding in vivo by the multivalent construct relative to the monomeric form.

Biodistribution Study

To further investigate the localization of ^{64}Cu-DOTA-ZD-G1 and ^{64}Cu-DOTA-ZD-G2 in U-87 MG tumor–bearing mice, we performed biodistribution studies at 24 h after injection immediately after the small-animal PET scans. The accumulation of ^{64}Cu-DOTA-ZD-G2 was slightly higher than that of ^{64}Cu-DOTA-ZD-G1 in the liver and gastrointestinal tract (Fig. 7), possibly due to differences in molecular weight or higher hydrophobicity. The measured tumor uptake of ^{64}Cu-DOTA-ZD-G2 (3.80 ± 0.22 %ID/g) was approximately 4 times higher than that of ^{64}Cu-DOTA-ZD-G1 (1.12 ± 0.07 %ID/g). Competition performed with ^{64}Cu-DOTA-ZD-G2 and 50 nmol of nonradioactive ZD-G2 decreased tumor uptake to 0.96 ± 0.03 %ID/g, which was approximately 3 times lower than mice imaged without cold compound ($P < 0.0001$). The excess amount of ZD-G2 reduced the uptake of ^{64}Cu-DOTA-ZD-G2 in U-87 MG tumors, whereas the radioactivity in the kidney and all other harvested tissues was not significantly increased in the presence or absence of nonradioactive competitor, except for the liver. Interestingly, the uptake of ^{64}Cu-DOTA-ZD-G1 in the liver was 1.68 ± 0.22 %ID/g, compared with 3.09 ± 0.07 %ID/g for ^{64}Cu-DOTA-ZD-G2, which increased to 5.63 ± 0.52 %ID/g with cold competitor, suggesting the presence of a low-affinity mechanism for hepatic uptake. Overall, these results demonstrate excellent tumor uptake of ^{64}Cu-DOTA-ZD-G2, with good agreement between the biodistribution data and that of semiquantitative ROI analysis by PET imaging.

DISCUSSION

An accurate assessment of VEGFR expression is crucial for the selection of patients who may benefit from VEGFR-targeted therapies. Here we describe the development and optimization of a PET radiopharmaceutical based on a small-molecule receptor tyrosine kinase inhibitor approved for clinical use, ZD6474 (vandetanib). We have shown that the dimeric constructs, ZD-G2 and ^{64}Cu-DOTA-ZD-G2, exhibit subnanomolar VEGFR affinity and specificity in vitro. This increased affinity corresponds to superior tumor accumulation in preclinical murine xenograft tumor models. Previously, we described the successful employment of multivalency strategies to develop a series of small-molecule imaging probes specific for $\alpha_v\beta_3$ integrins with enhanced affinity (*33,34*). Leveraging these earlier findings, we have applied a similar approach to develop a series of radiopharmaceuticals to target key cellular receptors guided, in part, by known structure–activity relationships of commercially available drugs. In this study, we used a triethanolamine linker to generate a dimeric derivative of ZD6474, which proved to be highly effective in improving VEGFR affinity. Chemical and structural properties of linkers may have significant effects on receptor affinity, pharmacokinetics, or biodistribution; however, the triethanolamine used in this work yielded favorable characteristics well suited for molecular imaging. We postulate that the flexibility of the C-O and C-N bonds in the linker permits acceptable interaction with the probe and binding sites of the receptor. Moreover, the N and O atoms in the linker may also increase the water-solubility of the dimeric complex, which is expected to affect its pharmacokinetic properties.

We examined the binding of ^{64}Cu-DOTA-ZD-G2 to cultured cells in 4 lines that differentially express this VEGFR. We have found that cell uptake of ^{64}Cu-DOTA-ZD-G2 was proportional to the levels of VEGFR expression in these cell lines (Figs. 2A and 2B). ^{64}Cu-DOTA-ZD-G2 demonstrated higher accumulation in U-87 cells than ^{64}Cu-DOTA-ZD-G1, and this effect was reversible by competition with nonradioactive compound (ZD-G2), strongly supporting receptor specificity (Fig. 2C). Binding studies with U-87 cells revealed a K_d of 0.45 nM for ^{64}Cu-DOTA-ZD-G2 and 44.7 nM for ^{64}Cu-DOTA-ZD-G1, representing approximately 2 orders of magnitude greater affinity of the dimeric configuration over the monomeric form. This improved affinity correlates with greater tumor uptake in murine xenograft models (Figs. 3 and 4).

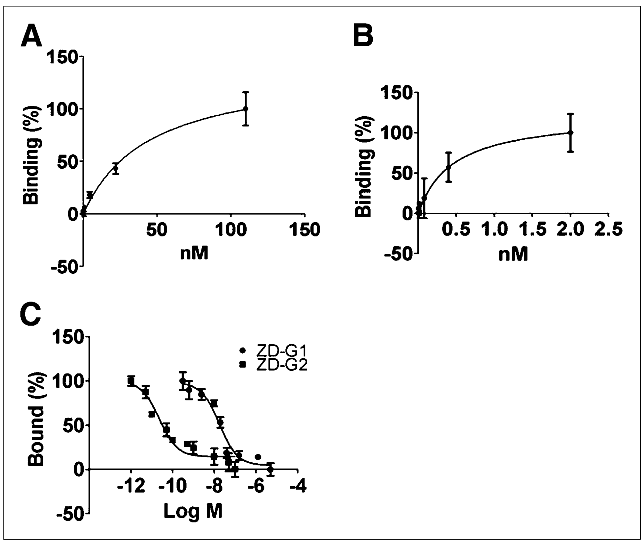

FIGURE 3. Characterization of VEGFR2-specific binding. (A) Saturation curve of ^{64}Cu-DOTA-ZD-G1 bound to U-87 cells (K_d, 44.75 ± 15.04 nM). (B) Saturation curve of ^{64}Cu-DOTA-ZD-G2 bound to U-87 cells. (K_d, 0.45 ± 0.32 nM. (C) Competition-binding curve of ^{64}Cu-DOTA-ZD-G2 and ^{64}Cu-DOTA-ZD-G1 to U-87 cells. Log of concentration of competitor compounds versus percentage of maximum specific binding of radiolabeled molecules.

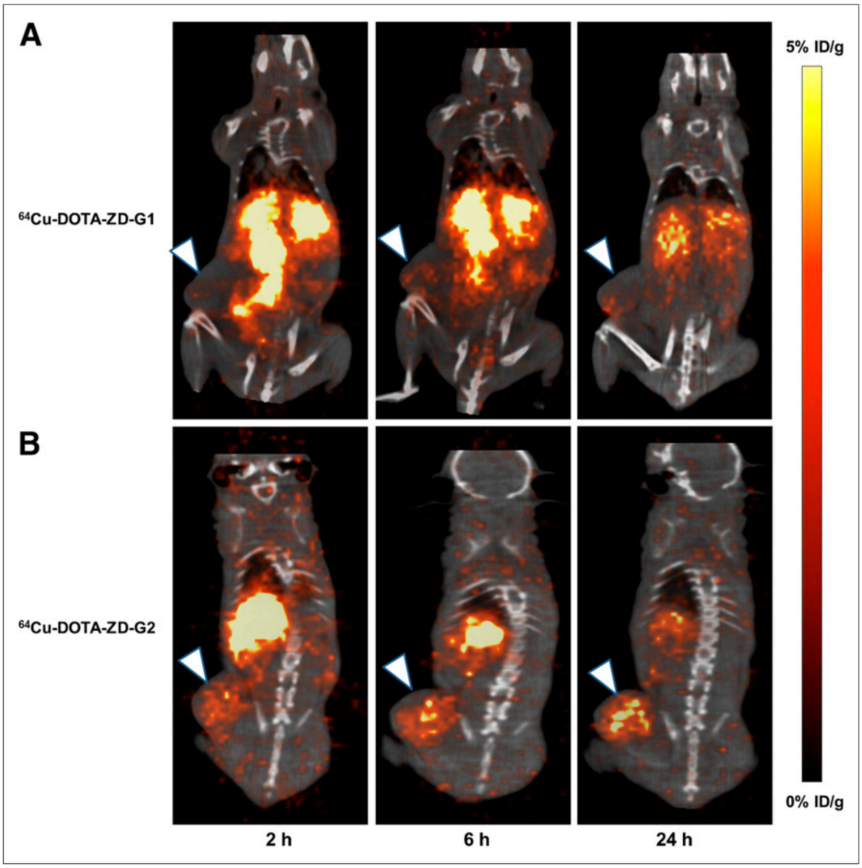

FIGURE 4. Small-animal PET/CT imaging of U-87 tumor–bearing mice. Serial small-animal PET/CT scans of U-87 tumor–bearing mice injected intravenously with approximately 3.7 MBq of ^{64}Cu-DOTA-ZD-G1 (A) and ^{64}Cu-DOTA-ZD-G2 (B). Tumors are indicated by arrowheads.

Small-animal PET imaging with ^{64}Cu-DOTA-ZD-G2 demonstrated significantly greater tumor uptake of up to 5-fold relative to that of ^{64}Cu-DOTA-ZD-G1 (Fig. 6A). Semiquantitative analysis revealed higher ^{64}Cu-DOTA-ZD-G2 uptake in U-87 tumors at all time points and greater tumor retention. The higher tumor uptake of ^{64}Cu-DOTA-ZD-G2 may be attributed to higher VEGFR binding affinity, longer circulation time, or slower tumor washout, compared with the monomeric ^{64}Cu-DOTA-ZD-G1. When compared with normal tissue, quantification of tumor-to-muscle ratios gave analogous results (Fig. 6B). Kidney localization of ^{64}Cu-DOTA-ZD-G2 was low at all time points, representing an advantage over biologics-based imaging agents that often exhibit high renal activity. Liver uptake of ^{64}Cu-DOTA-ZD-G2 was initially high at 2 h after injection (15.7 %ID/g) but rapidly cleared (3.9 %ID/g) by 24 h, a favorable property for PET imaging. These findings support the successful development of a PET radiopharmaceutical derived from a small-molecule VEGFR inhibitor using multivalency to synergistically improve receptor affinity while maintaining distribution and pharmacokinetic properties favorable for clinical translation.

Although the improved receptor affinity clearly affected imaging, the resulting dimeric form of ZD6474 may also be tested for improved antitumor effects either as a nonradioactive compound or as a β-particle–emitting theranostic agent. We have already begun to explore this promising approach to our theranostics development efforts. From a commercialization standpoint, the ^{64}Cu chelator–based radiopharmaceutical configuration will allow for greater clinical use because it obviates the need for an on-site cyclotron. Radiopharmaceutical kits would be possible with on-demand ^{64}Cu conjugation to be performed at nuclear medicine facilities, and the relatively long half-life of ^{64}Cu (12.7 h) permits long-range shipping options. For therapeutic applications, the use of a DOTA-compatible β-particle–emitting radioisotope, including ^{90}Y, is also both practical and commercially feasible.

CONCLUSION

We have developed a high-affinity PET radiopharmaceutical, ^{64}Cu-DOTA-ZD-G2, based on the commercially available Food and Drug Administration–approved oncologic drug vandetanib (ZD6474), to noninvasively image VEGFR in a murine xenograft tumor model. By leveraging the synergistic effects of multivalency, we synthesized a dimeric form of vandetanib using a suitable linker to couple a chelator for ^{64}Cu that yielded subnanomolar binding to VEGFR. This compound demonstrated approximately 2 orders of magnitude improvement in VEGFR binding affinity in vitro, compared with the monomeric form, and significantly enhanced tumor localization, with excellent biodistribution and pharmacokinetic properties for clinical translation and potential commercialization.

These results suggest that ^{64}Cu-DOTA-ZD-G2 may be used as a companion diagnostic molecular imaging agent for the detection of VEGFR overexpression to assist in patient selection and response monitoring for targeted therapy. Moreover, the improved receptor affinity of the dimeric compound suggests a robust platform for producing next-generation drugs based on parent compounds that have relatively poor receptor targeting. Our findings raise the possibility of using the dimeric form of vandetanib (ZD-G2) as a nonradioactive drug

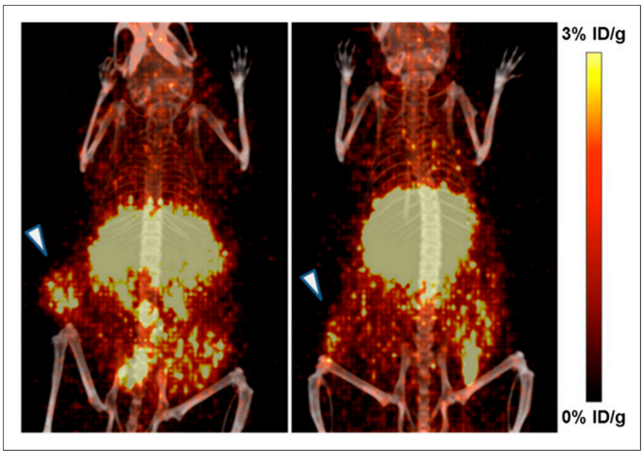

FIGURE 5. Representative whole-body PET/CT images of U-87 MG tumor–bearing mice at 24 h after injection of ^{64}Cu-DOTA-ZD-G2 (left) and ^{64}Cu-DOTA-ZD-G2 coinjected with 60 μg of ZD-G2 (right). Tumors are indicated by arrowheads.

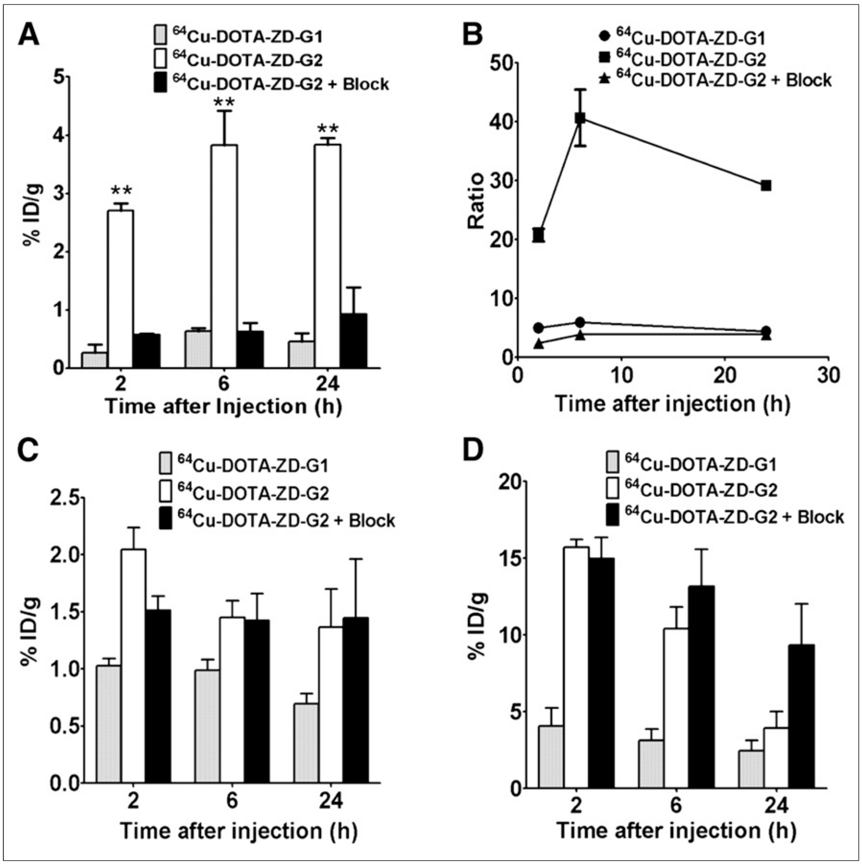

FIGURE 6. Quantitative analysis of small-animal PET/CT scans. Comparison of decay-corrected ROI analysis of ^{64}Cu-DOTA-ZD-G1, ^{64}Cu-DOTA-ZD-G2, and ^{64}Cu-DOTA-ZD-G2 with coinjection of 60 μg of ZD-G2 in tumor (A), kidneys (C), and liver (D) ($n = 5$, $^{**}P < 0.0001$). (B) Comparison of tumor-to-muscle uptake ratios after injection of ^{64}Cu-DOTA-ZD-G1, ^{64}Cu-DOTA-ZD-G2, and ^{64}Cu-DOTA-ZD-G2 with coinjection of 60 μg of ZD-G2. Data shown represent mean ± SD ($n = 5$ per group).

with subnanomolar receptor affinity or as a therapeutic agent using DOTA-ZD-G2 coupled to a β-emitting radionuclide such as ^{90}Y. Further work in this exciting theranostic platform is under way.

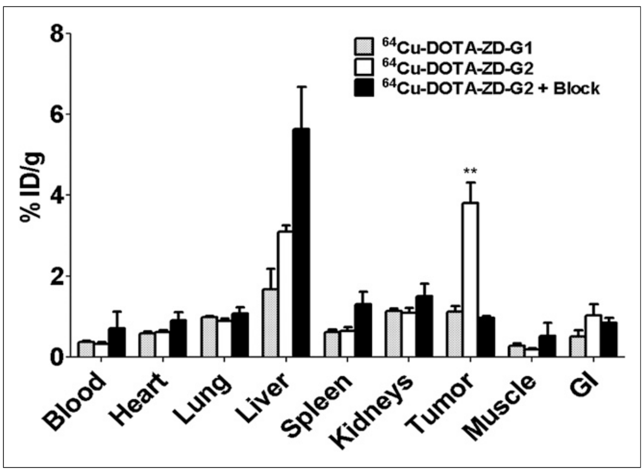

FIGURE 7. Biodistribution at 24 h after injection of ^{64}Cu-DOTA-ZD G1, ^{64}Cu-DOTA-ZD-G2, and ^{64}Cu-DOTA-ZD-G2 with coinjection of 60 μg of ZD-G2 in U-87 tumor–bearing mice. Data shown represent mean ± SD ($^{**}P < 0.0001$, $n = 5$ per group).

DISCLOSURE

The costs of publication of this article were defrayed in part by the payment of page charges. Therefore, and solely to indicate this fact, this article is hereby marked “advertisement” in accordance with 18 USC section 1734. This work was funded by Houston Methodist Research Institute. No other potential conflict of interest relevant to this article was reported.

ACKNOWLEDGMENT

We thank the small-animal imaging core at Houston Methodist Research Institute for the small-animal PET/CT imaging.

REFERENCES

1. Ferrara N, Gerber HP, LeCouter J. The biology of VEGF and its receptors. *Nat Med.* 2003;9:669–676.
2. Folkman J. Angiogenesis: an organizing principle for drug discovery? *Nat Rev Drug Discov.* 2007;6:273–286.
3. Baluk P, Hashizume H, McDonald DM. Cellular abnormalities of blood vessels as targets in cancer. *Curr Opin Genet Dev.* 2005;15:102–111.
4. Simons M. Angiogenesis: where do we stand now? *Circulation.* 2005;111:1556–1566.
5. Ferrara N, Hillan KJ, Gerber HP, Novotny W. Discovery and development of bevacizumab, an anti-VEGF antibody for treating cancer. *Nat Rev Drug Discov.* 2004;3:391–400.
6. Olsson AK, Dimberg A, Kreuger J, Claesson-Welsh L. VEGF receptor signaling: in control of vascular function. *Nat Rev Mol Cell Biol.* 2006;7:359–371.
7. Underiner TL, Ruggeri B, Gingrich DE. Development of vascular endothelial growth factor receptor (VEGFR) kinase inhibitors as anti-angiogenic agents in cancer therapy. *Curr Med Chem.* 2004;11:731–745.
8. Awasthi N, Schwarz MA, Verma V, Cappiello C, Schwarz RE. Endothelial monocyte activating polypeptide II interferes with VEGF-induced proangiogenic signaling. *Lab Invest.* 2009;89:38–46.
9. Roskoski R. Vascular endothelial growth factor (VEGF) signaling in tumor progression. *Crit Rev Oncol Hematol.* 2007;62:179–213.
10. Takahashi Y, Kitadai Y, Bucana CD, Cleary KR, Ellis LM. Expression of vascular endothelial growth-factor and its receptor, kdr, correlates with vascularity, metastasis, and proliferation of human colon-cancer. *Cancer Res.* 1995;55:3964–3968.
11. Pàez-Ribes M, Allen E, Hudock J, et al. Antiangiogenic therapy elicits malignant progression of tumors to increased local invasion and distant metastasis. *Cancer Cell.* 2009;15:220–231.
12. Bergers G, Hanahan D. Modes of resistance to anti-angiogenic therapy. *Nat Rev Cancer.* 2008;8:592–603.
13. Schenone S, Bondavalli F, Botta M. Antiangiogenic agents: an update on small molecule VEGFR inhibitors. *Curr Med Chem.* 2007;14:2495–2516.
14. Kniess T. Radiolabeled small molecule inhibitors of VEGFR: recent advances. *Curr Pharm Des.* 2012;18:2867–2874.
15. Chau NG, Haddad RI. Vandetanib for the treatment of medullary thyroid cancer. *Clin Cancer Res.* 2013;19:524–529.
16. Tolmachev V, Stone-Elander S, Orlova A. Radiolabelled receptor-tyrosine-kinase targeting drugs for patient stratification and monitoring of therapy response: prospects and pitfalls. *Lancet Oncol.* 2010;11:992–1000.
17. Hicks JW, VanBrocklin HF, Wilson AA, Houle S, Vasdev N. Radiolabeled small molecule protein kinase inhibitors for imaging with PET or SPECT. *Molecules.* 2010;15:8260–8278.
18. Foersch S, Kiesslich R, Waldner MJ, et al. Molecular imaging of VEGF in gastrointestinal cancer in vivo using confocal laser endomicroscopy. *Gut.* 2010; 59:1046–1055.

19. Hao G, Hajibeigi A, Leon-Rodriguez LM, Oz OK, Sun X. Peptoid-based PET imaging of vascular endothelial growth factor receptor (VEGFR) expression. *Am J Nucl Med Mol Imaging.* 2011;1:65–75.
20. Michalski MH, Chen X. Molecular imaging in cancer treatment. *Eur J Nucl Med Mol Imaging.* 2011;38:358–377.
21. Nagengast WB, De Korte MA, Oude Munnink TH, et al. ^{89}Zr-bevacizumab PET of early antiangiogenic tumor response to treatment with HSP90 inhibitor NVP-AUY922. *J Nucl Med.* 2010;51:761–767.
22. van der Bilt AR, Terwisscha van Scheltinga AG, Timmer-Bosscha H, et al. Measurement of tumor VEGF-A levels with Zr-89-bevacizumab PET as an early biomarker for the antiangiogenic effect of everolimus treatment in an ovarian cancer xenograft model. *Clin Cancer Res.* 2012;18:6306–6314.
23. Scheer MG, Stollman TH, Boerman OC, et al. Imaging liver metastases of colorectal cancer patients with radiolabelled bevacizumab: lack of correlation with VEGF-A expression. *Eur J Cancer.* 2008;44:1835–1840.
24. Jayson GC, Zweit J, Jackson A, et al. Molecular imaging and biological evaluation of HuMV833 anti-VEGF antibody: implications for trial design of antiangiogenic antibodies. *J Natl Cancer Inst.* 2002;94:1484–1493.
25. Rodriguez-Porcel M, Cai W, Gheysens O, et al. Imaging of VEGF receptor in a rat myocardial infarction model using PET. *J Nucl Med.* 2008;49:667–673.
26. Cai W, Chen K, Mohamedali KA, et al. PET of vascular endothelial growth factor receptor expression. *J Nucl Med.* 2006;47:2048–2056.
27. Chen K, Cai W, Li ZB, Wang H, Chen X. Quantitative PET imaging of VEGF receptor expression. *Mol Imaging Biol.* 2009;11:15–22.
28. Wang H, Cai W, Chen K, et al. A new PET tracer specific for vascular endothelial growth factor receptor 2. *Eur J Nucl Med Mol Imaging.* 2007;34:2001–2010.
29. Flanigan J, Deshpande H, Gettinger S. Current status of vandetanib (ZD6474) in the treatment of non-small cell lung cancer. *Biologics.* 2010;4:237–243.
30. Samén E, Thorell JO, Lu L, Tegnebratt T, Holmgren L, Stone-Elander S. Synthesis and preclinical evaluation of [^{11}C]PAQ as a PET imaging tracer for VEGFR-2. *Eur J Nucl Med Mol Imaging.* 2009;36:1283–1295.
31. Hennequin LF, Stokes ESE, Thomas AP, et al. Novel 4-anilinoquinazolines with C-7 basic side chains: Design and structure activity relationship of a series of potent, orally active, VEGF receptor tyrosine kinase inhibitors. *J Med Chem.* 2002;45:1300–1312.
32. Meng Q, Li F, Jiang S, Li Z. Novel ^{64}Cu-labeled CUDC-101 for in vivo PET imaging of histone deacetylases. *ACS Med Chem Lett.* 2013;4:858–862.
33. Li F, Jas GS, Qin G, Li K, Li Z. Synthesis and evaluation of bivalent, peptidomimetic antagonists of the αvβ3 integrins. *Bioorg Med Chem Lett.* 2010;20:6577–6580.
34. Li F, Liu J, Jas GS, et al. Synthesis and evaluation of a near-infrared fluorescent non-peptidic bivalent integrin $\alpha_v\beta_3$ antagonist for cancer imaging. *Bioconjug Chem.* 2010;21:270–278.